

Effect of lanthanide promotion on catalytic performance of sol–gel Ni/Al₂O₃ catalysts in steam reforming of propane

Sittichai Natesakhawat, Okan Oktar, Umit S. Ozkan*

The Ohio State University, Department of Chemical and Biomolecular Engineering, 140 W, 19th Avenue, Columbus, OH 43210, USA

Received 26 April 2005; received in revised form 7 July 2005; accepted 7 July 2005

Available online 16 August 2005

Abstract

The effect of lanthanide elements (La, Ce, and Yb) on the catalytic behavior of sol–gel Ni/Al₂O₃ catalysts in propane steam reforming was investigated. Steady-state reaction experiments show that the addition of small amounts (2 wt.%) of lanthanide elements improves the catalytic activity and stability significantly. The changes in reaction performance are related to catalyst reducibility, nickel surface area and resistance to deactivation. Temperature-programmed reduction (TPR) and X-ray photoelectron spectroscopy (XPS) characterization results reveal that the presence of lanthanide elements enhances the catalyst reducibility; the positive effect is most evident with 20% Ni–2% Ce/Al₂O₃ catalysts. H₂ chemisorption data indicate that 20% Ni–2% Ce/Al₂O₃ catalysts exhibit larger nickel surface area compared to 20% Ni/Al₂O₃ catalysts. Nickel surface area of sol–gel catalysts is also found to be strongly dependent on calcination and reduction temperatures. In situ DRIFTS experiments coupled with TPD and TPR reaction suggest that formate and carbonate species are formed upon the reaction of adsorbed propane and water on reduced catalysts.

© 2005 Elsevier B.V. All rights reserved.

Keywords: Steam reforming; Propane; Ni/Al₂O₃ catalysts; Sol–gel; Lanthanides; H₂ chemisorption; DRIFTS

1. Introduction

Hydrogen is the ultimate clean energy carrier. When it is combusted, heat and water are the only products. When it is used as a fuel for fuel cells, then it has the potential of providing much higher efficiencies compared to combustion. Thus, hydrogen offers a potentially non-polluting and efficient fuel for today's rising energy demands [1]. However, in the transition period before renewable sources of hydrogen can be developed, production of hydrogen from fossil fuels remains an important technology. Currently, steam reforming of natural gas, which is composed mainly of methane, is used to produce most of hydrogen in US and about half of the world's hydrogen supply. Naphtha fractions with a final boiling point of less than 220 °C are also considered as suitable feedstocks for hydrogen production [2]. However, current Ni-based catalysts, which are used for natural gas

steam reforming processes, suffer from catalyst deactivation by coke formation more severely when higher hydrocarbons are reformed at low steam/carbon ratios.

Although supported precious metals such as Pd, Pt, and Rh have been reported to be active and stable for steam reforming of hydrocarbons [3–8], the cost of the precious metals is still a major drawback. The low-cost and long-proven performance of Ni-based catalysts, therefore, warrant the effort to optimize these catalysts for steam reforming applications, particularly fuel processing technology from existing liquid fuels such as gasoline and diesel.

There is evidence in the literature pointing to an improvement in catalytic activity of Ni-based catalysts in hydrocarbon steam reforming with the addition of lanthanide elements [9–11]. Zhuang et al. [9] investigated the effect of cerium oxide as a promoter in supported Ni catalysts for methane steam reforming. It showed a beneficial effect by not only decreasing the carbon deposition rate, but also increasing the steam reforming activity. The authors believed that cerium oxide accelerated the reaction of steam with

* Corresponding author. Tel.: +1 614 292 6623; fax: +1 614 292 3769.
E-mail address: ozkan.1@osu.edu (U.S. Ozkan).

adsorbed species on the nickel surface, thus decreasing the carbon deposition as well as increasing or maintaining the catalytic activity. Su and Guo [10] also reported an improvement in catalytic activity and resistance to Ni sintering of Ni/Al₂O₃ catalysts doped with rare earth oxides in methane steam reforming. The growth of Ni particles and the formation of inactive NiO and NiAl₂O₄ phases were suppressed by the addition of rare earth oxides. Moreover, the oxides of heavy rare earth elements (Gd, Er, Dy) exhibited a more pronounced effect than those of the light ones (La, Pr, Nd).

The use of lanthanide-promoted Ni/Al₂O₃ catalysts in dry reforming of methane [12–15] and benzene hydrogenation [16] has also been reported. The effects of the addition of lanthanide oxides (La₂O₃ and CeO₂) and preparation procedures were investigated in the reforming of methane with carbon dioxide over impregnated Ni/Al₂O₃ catalysts [12]. When lanthanides were impregnated prior to nickel, an enhanced reducibility of nickel and a decrease in nickel particle size were observed. However, the reforming activity was not affected to a large extent by the impregnation order of nickel and lanthanides. The presence of CeO₂ (1–5 wt.%) in impregnated Ni/ γ -Al₂O₃ catalysts was found to reduce the chemical interaction between nickel and the alumina support, resulting in an increase in reducibility and higher nickel dispersion [13,14]. Moreover, carbon deposition was greatly suppressed due to the oxygen storage capacity of CeO₂. The catalytic activity, sulfur tolerance, and thermal stability were remarkably improved after adding La, Sm, and Yb into Ni-B/Al₂O₃ catalysts for benzene hydrogenation [16]. The positive effect of lanthanide promotion was associated with easier reduction of nickel oxides, smaller nickel particles, and larger surface area of active nickel.

In this study, Ni/Al₂O₃ catalysts promoted with lanthanide elements (La, Ce, and Yb) were prepared by a modified sol–gel technique and were examined in propane steam reforming. Characterization was performed using the BET N₂ adsorption method, X-ray diffraction (XRD), temperature-programmed reduction (TPR), X-ray photoelectron spectroscopy (XPS), and H₂ chemisorption. In situ DRIFTS studies were also conducted to identify adsorbed species under C₃H₈ and C₃H₈+H₂O flows as well as to elucidate the reaction pathways for propane steam reforming.

2. Experimental

2.1. Catalyst preparation

Catalysts were prepared using a modified sol–gel technique. Nickel and lanthanide precursors (Aldrich) used were in nitrate form. For the aluminum precursor, aluminum tri-*sec*-butoxide (ATB; Aldrich) was used. Ethanol (Alfa Aesar; 130 cm³) was used as the solvent. The following sol–gel

parameters were varied during the synthesis: nickel content = 10–25 wt.%, lanthanide content = 2–5 wt.%, H₂O/ATB molar ratio = 3.6–5.0, and pH of the resulting gels = 4.8–8.5. Initially, ATB was placed in ethanol and stirred. The aqueous solutions with the desired amounts of nickel and lanthanide were added dropwise into the suspension using a syringe pump at the flow rate of 0.5 cm³/min. It is noted that the aqueous lanthanide nitrate solution was added first followed by that of nickel. The pH of the resulting green gel was measured and adjusted by adding HNO₃ (Fisher) or NH₄OH (Fisher). The gels were stirred for an additional 15 min and were kept at room temperature for 30 min. The samples were then dried overnight in the oven at 110 °C to remove the remaining water and ethanol. The dry samples were ground to a fine powder and were calcined under O₂ at 450 °C (ramp rate = 10 °C/min) for 4 h.

2.2. Catalyst characterization

BET surface areas of calcined catalysts were measured by N₂ adsorption–desorption at 77 K using a Micromeritics ASAP 2010 instrument. Before measurements, samples were degassed under vacuum at 130 °C overnight. XRD patterns of calcined and reduced catalysts were obtained with a Bruker D8 Advance X-ray diffractometer equipped with atmosphere and temperature control stage and using Cu K α radiation ($\lambda = 1.542 \text{ \AA}$) operated at 40 kV and 50 mA. In this experiment, 5% H₂/N₂ was used as a reducing agent. TPR of catalysts was conducted using a laboratory-made gas flow system described in detail elsewhere [17]. Catalyst samples (50 mg) were placed in a 1/4 in. o.d. quartz U-tube reactor. The catalysts were then re-calcined under 10% O₂/He at 450 °C for 1 h followed by cooling to room temperature under Ar. The reduction was performed with 10% H₂/Ar (40 cm³ (STP)/min). The temperature of the catalysts was raised using a ramp rate of 10 °C/min to 900 °C and held at that level for 10 min. The effluent from the reactor was passed through a silica gel water trap to remove moisture formed during reduction. H₂ consumption was measured using a thermal conductivity detector (TCD) connected to a data-acquisition computer.

XPS of reduced catalysts was performed with an AXIS Ultra XPS spectrometer with an Al anode operated at 14 kV and 10 mA. Reduction was performed with 20% H₂/N₂ at 600 °C for 2 h. Prior to the measurements, all reduced catalysts were kept in tightly sealed reactors and were subsequently mounted on a sample holder with conductive tape in a dry glovebox filled with Ar. The sample holder was then carefully transferred to the analysis chamber of the spectrometer with a controlled-atmosphere transporter. Spectra were corrected using the C 1s signal located at 284.5 eV.

H₂ chemisorption of catalysts was conducted using a Micromeritics ASAP 2010 Chemisorption System. Prior to adsorption measurements, calcined samples (0.2 g) were reduced under H₂ at the desired reduction temperature for 2 h. Subsequently, the samples were cooled down to 35 °C

followed by evacuation to 10^{-5} mmHg. The adsorption isotherms were measured at equilibrium pressures between 50 and 500 mmHg. H_2 uptakes at monolayer coverage of the Ni crystallites were used to estimate Ni dispersion and metallic surface area, assuming that each surface Ni atom chemisorbs one hydrogen atom ($H/Ni_{\text{surface}} = 1$).

DRIFTS experiments were performed using a Bruker IFS66 instrument equipped with an MCT detector and a KBr beamsplitter. Catalysts were reduced under 20% H_2/N_2 at 600 °C for 2 h and then were placed in a sample cup inside a Spectratech diffuse reflectance cell equipped with KBr windows and a thermocouple that allowed direct measurements of the surface temperature. Spectra for each experiment were averaged over 1000 scans in the mid-IR range ($400\text{--}4000\text{ cm}^{-1}$) to a nominal 3 cm^{-1} resolution. Prior to the collection of spectra, the catalysts were re-reduced in situ under 20% H_2/He at 450 °C for 1 h. The background spectra were taken at different temperature intervals under He. The adsorption of C_3H_8 was performed at room temperature for 1 h followed by flushing under He for 30 min. The spectra were subsequently collected at different temperatures up to 450 °C.

2.3. Reaction studies

The steady-state reaction experiments were performed using a stainless steel fixed-bed flow reactor (1/4 in. o.d.). Catalysts were compared in propane steam reforming using equal surface area loading (9 m^2) in the reactor at 400–550 °C and $H_2O/C = 1.3$. The feed percentages for these experiments were $C_3H_8/H_2O/N_2 = 1/4/95$ (feed flow rate = 300–400 cm^3 (STP)/min). Unless otherwise noted, catalysts were reduced in situ under 20% H_2/N_2 (50 cm^3 (STP)/min) at 600 °C for 2 h prior to the reaction. The effluent from the reactor was analyzed using an automated Shimadzu GC-14A equipped with FID and TCD detectors. Separations were performed under Ar using two columns: Porapak Q (12 ft \times 1/8 in. SS, 80/100 mesh) and Molecular Sieve 13X (5 ft \times 1/8 in. SS, 60/80 mesh). A GOW-MAC 069-50 ruthenium methanizer operated at 350 °C was used with the FID for the sensitive determination of CO as low as 10 ppm. Reaction data were taken after steady state was reached. Conversion, yield, and selectivities were defined as follows:

$$\%C_3H_8 \text{ conversion} = \left(\frac{\text{moles of carbon converted}}{\text{total moles of carbon in the feed}} \right) \times 100$$

$$\%H_2 \text{ yield} = \left(\frac{2 \times \text{moles of } H_2 \text{ produced}}{\text{total moles of hydrogen in the feed}} \right) \times 100$$

%C-product selectivity for A

$$= \left(\frac{\text{moles of C in product A}}{\text{moles of C in all carbon - containing products}} \right) \times 100$$

%H-product selectivity for B

$$= \left(\frac{\text{moles of H in product B}}{\text{moles of H in all H - containing products}} \right) \times 100$$

C-containing products are CO, CO_2 , and CH_4 . H-containing products are H_2 and CH_4 . Reproducibility of the results were tested using different catalyst batches run under identical conditions.

3. Results and discussion

3.1. Physical properties of sol-gel catalysts

The effect of synthesis parameters on the physical properties of sol-gel Ni/Al_2O_3 catalysts is reported in Table 1. Parameters that were varied during the synthesis included Ni content, pH of the resulting gels, and H_2O/ATB molar ratio. BET surface area of sol-gel Ni/Al_2O_3 catalysts is seen to decrease with increasing Ni contents possibly due to nickel aggregation to form larger particles on the Al_2O_3 support surface during thermal treatment. The decrease in surface area is even more pronounced at higher Ni contents. Furthermore, an increase in pH and H_2O/ATB ratio causes an increase in surface area of 20 wt.% Ni/Al_2O_3 catalysts. It is noted that a decrease in the pore diameter from 10.5 to 7.4 nm occurs when H_2O/ATB ratio is increased from 3.6 to 5.0. This phenomenon is related to an increase in cross-linking as a result of an increase in the extent of hydrolysis at high H_2O/ATB ratios [18].

BET surface areas of lanthanide-promoted sol-gel Ni/Al_2O_3 catalysts prepared at different lanthanide contents are listed in Table 2. In general, catalysts have a lower surface area than the pure support. At lower loading levels, the lanthanide-promoted catalysts exhibit a higher surface area than the unpromoted catalyst, but a loss in surface area with higher lanthanide content is observed with $Ni-Ce/Al_2O_3$ and $Ni-Yb/Al_2O_3$ catalysts possibly due to pore blockage by excess metal. In addition, an increase in calcination temperature from 450 to 600 °C causes a decrease in surface area

Table 1
BET surface area of various sol-gel Ni/Al_2O_3 catalysts

Synthesis parameters			Surface area (m^2/g)
Ni content (wt%)	pH	H_2O/ATB ratio	
10	4.8	3.6	248
15	4.8	3.6	244
20	4.8	3.6	209
25	4.8	3.6	180
20	4.8	3.6	209
20	7.0	3.6	215
20	8.8	3.6	259
20	4.8	3.6	209
20	4.8	4.0	203
20	4.8	5.0	248

Table 2

BET surface area of lanthanide-promoted sol-gel Ni/Al₂O₃ catalysts calcined at 450 °C

Catalyst	Surface area (m ² /g)
20% Ni/Al ₂ O ₃	209
20% Ni–2% La/Al ₂ O ₃	286
20% Ni–5% La/Al ₂ O ₃	300
20% Ni–2% Ce/Al ₂ O ₃	304
20% Ni–5% Ce/Al ₂ O ₃	228
20% Ni–2% Yb/Al ₂ O ₃	278
20% Ni–5% Yb/Al ₂ O ₃	234
Al ₂ O ₃	342

of Ni–Ce/Al₂O₃ catalysts. The surface area of the catalyst calcined at 600 °C is 261 m²/g compared to 304 m²/g for the catalyst calcined at 450 °C.

3.2. X-ray diffraction

The XRD patterns of calcined and reduced 20% Ni–2% Ce/Al₂O₃ catalysts are compared in Fig. 1. The support calcined at 450 °C is relatively amorphous as evidenced by broad peaks that correspond to γ -Al₂O₃ (Fig. 1a). The possible crystalline phases in the catalyst calcined at 450 °C are NiO, NiAl₂O₄, and γ -Al₂O₃ (Fig. 1b). However, XRD results are not conclusive about the presence of any Ni-containing crystalline phases, suggesting a high-level of dispersion of Ni. Furthermore, no cerium-related crystalline phases are detected, suggesting that cerium species could be well dispersed over the alumina support or could exist within the NiO matrix undetectable by XRD. After in situ reduction under 5% H₂/N₂ at 600 °C, significant amounts of metallic nickel were formed as confirmed by the diffraction lines of a metallic nickel phase [(1 1 1), (2 0 0), (2 2 0)] at $2\theta = 44.5^\circ$, 51.8° , and 76.4° , respectively (Fig. 1c).

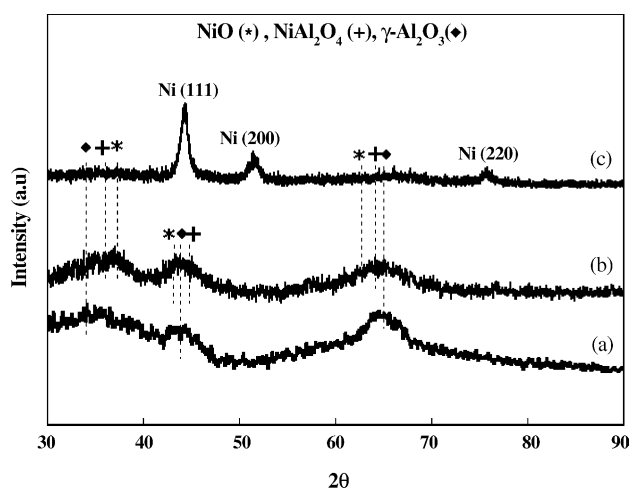


Fig. 1. XRD patterns of (a) sol-gel Al₂O₃ calcined at 450 °C (b) 20% Ni–2% Ce/Al₂O₃ catalyst calcined at 450 °C (c) 20% Ni–2% Ce/Al₂O₃ catalyst reduced at 600 °C.

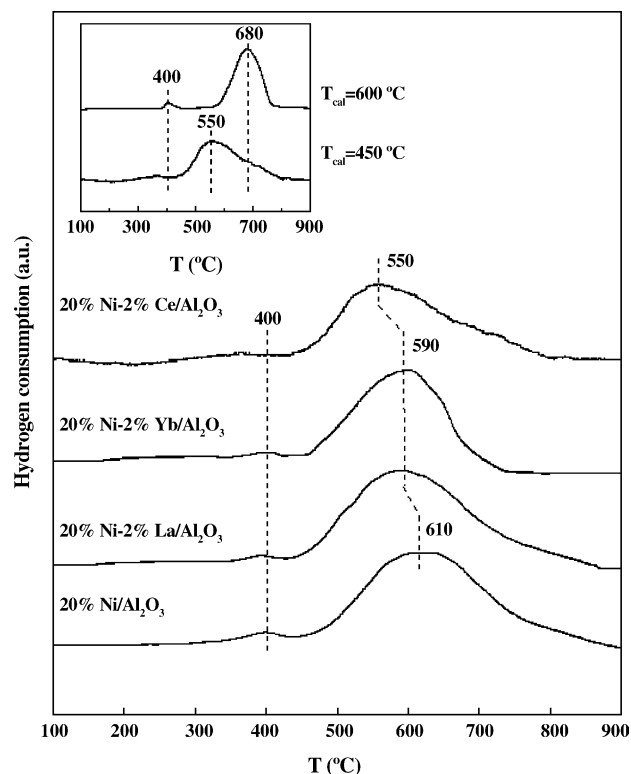


Fig. 2. TPR profiles of various sol-gel 20% Ni/Al₂O₃ catalysts promoted with 2 wt.% lanthanide elements (calcined at 450 °C). The effect of calcination temperature on reducibility of 20% Ni–2% Ce/Al₂O₃ catalysts is shown as an inset.

3.3. Promotion effect on catalyst reducibility and nickel surface area

3.3.1. Temperature-programmed reduction

TPR experiments on lanthanide-promoted sol-gel Ni/Al₂O₃ catalysts were performed using 10% H₂/Ar as a reducing agent. As shown in Fig. 2, the TPR profiles exhibit two peaks, representing two different reduction sites on all catalysts. A small low-temperature (LT) reduction peak around 400 °C could be assigned to the reduction of trace amounts of NiO clusters. A broad high-temperature (HT) reduction peak above 500 °C could be due to the reduction of a well-dispersed and possibly amorphous NiO phase that interacts strongly with the alumina support. For lanthanide-promoted catalysts calcined at 450 °C, the position of the HT peak maximum shifts toward lower temperatures compared to that of the unpromoted catalyst. This suggests that the presence of lanthanide elements results in a greater reduction of nickel species; the promotion effect is most evident on the Ni–Ce/Al₂O₃ catalyst. This could be due to a decreased interaction of Ni with the alumina support when a lanthanide element is present as a promoter. It is noted that the introduction of lanthanides to nickel catalysts showed no additional reduction peak under these conditions.

In general, calcination temperature plays a major role on the strength of metal oxide and support interaction for

supported metal catalysts, which in turn strongly affects the degree of reduction. The effect of calcination temperature on the catalyst reducibility of Ni–Ce/Al₂O₃ was also investigated. An increase in calcination temperature from 450 to 600 °C results in a shift of the HT peak maximum to a higher temperature around 680 °C as displayed in an inset (Fig. 2). Moreover, the reduction peak at 400 °C is more prominent with the catalyst calcined at 600 °C implying that the formation of crystalline NiO could be enhanced as the calcination temperature is increased. TPR results show that the interaction of Ni species with the alumina support becomes stronger at higher calcination temperatures, thus suppressing the reduction of Ni species to metallic Ni [19,20]. This could also be indicative of the formation of a nickel aluminate spinel at higher calcination temperatures.

3.3.2. X-ray photoelectron spectroscopy

XPS was further conducted to study the nature of surface nickel species over the catalysts after reduction under 20% H₂/N₂ at 600 °C for 2 h. The catalysts were transferred to the XPS chamber without exposing them to the atmosphere. The Ni 2p spectra of reduced lanthanide-promoted catalysts are shown in Fig. 3. The Ni 2p spectra of the catalysts exhibit features that are assigned to Ni²⁺ with Ni 2p_{3/2} and Ni 2p_{1/2} binding energies at 855.8 and 873.3 eV, respectively and Ni⁰ with Ni 2p_{3/2} and Ni 2p_{1/2} binding energies at 852.7 and

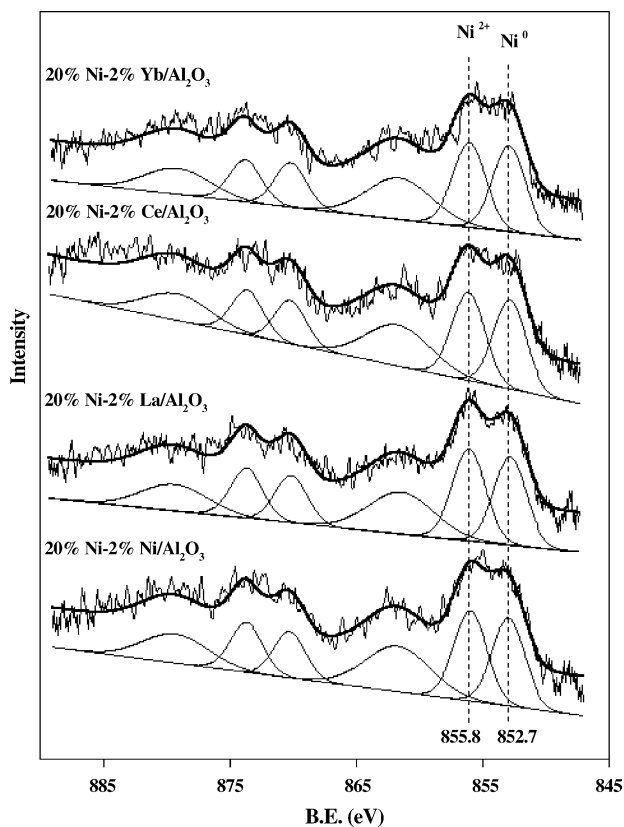


Fig. 3. Ni 2p X-ray photoelectron spectra of lanthanide-promoted sol-gel 20% Ni/Al₂O₃ catalysts reduced at 600 °C.

Table 3

Comparison of the $A_{\text{Ni}^0}/(A_{\text{Ni}^0} + A_{\text{Ni}^{2+}})$ XPS ratio of the catalysts after reduction at 600 °C

Catalyst	$A_{\text{Ni}^0}/(A_{\text{Ni}^0} + A_{\text{Ni}^{2+}})$
20% Ni/Al ₂ O ₃	0.51
20% Ni–2% La/Al ₂ O ₃	0.51
20% Ni–2% Ce/Al ₂ O ₃	0.55
20% Ni–2% Yb/Al ₂ O ₃	0.54

870.2 eV, respectively [21–24]. The Ni 2p_{3/2} signal corresponding to Ni²⁺ is accompanied by a broader peak located at 860.8 eV due to a strong shake-up process [25]. Ni 2p spectra indicate that the reduction of nickel species to the metallic state in the sol-gel catalysts is not complete due to a strong interaction of nickel oxide with the alumina support. It is noted that the satellite peak at 860.8 eV still remains in XPS spectra following TPR experiments (not shown). This suggests that the signal of Ni²⁺ species could be due to NiAl₂O₄, which is more difficult to reduce. However, the possibility of a NiO phase cannot be excluded since the Ni 2p binding energies for these two species are very close together. In addition, all catalysts show similar Ni 2p spectra, suggesting that nickel species in these catalysts exist in a similar coordination environment.

Deconvolution of the Ni 2p spectra was performed by Gaussian–Lorentzian curve-fitting method to determine the peak areas for obtaining relative surface concentrations of nickel species. The ratio of peak areas $A_{\text{Ni}^0}/(A_{\text{Ni}^0} + A_{\text{Ni}^{2+}})$ is used to illustrate the degree of reducibility. As displayed in Table 3, an increase in the $A_{\text{Ni}^0}/(A_{\text{Ni}^0} + A_{\text{Ni}^{2+}})$ ratio for lanthanide-promoted Ni/Al₂O₃ catalysts is seen after reduction compared to that of the unpromoted catalyst, indicative of an enhancement in the catalyst reducibility with lanthanide promotion. This is in agreement with TPR results obtained with the lanthanide-promoted catalysts, which have shown a shift in the maximum of the high-temperature peak corresponding to the reduction of NiO toward lower temperatures.

3.3.3. H₂ chemisorption

H₂ chemisorption was performed to determine nickel dispersion and nickel surface area of the catalysts. Unless otherwise noted, the reduction was conducted under H₂ (UHP, 99.999%) at 600 °C for 2 h. The catalysts were then evacuated at 610 °C to remove adsorbed hydrogen from the surface and cooled to 35 °C. The first analysis was performed to measure both strong and weak sorption in combination whereas a repeat analysis was conducted to measure only weak (reversible) hydrogen uptake. The difference in the volume of hydrogen adsorbed from the first and repeat analyses was then plotted versus the hydrogen pressure and was extrapolated to zero pressure to obtain hydrogen uptake due to chemisorption on nickel. The nickel dispersion and nickel surface area were calculated assuming that one hydrogen atom is adsorbed on one surface nickel atom [26–28].

As listed in Table 4, the nickel dispersion is observed to be quite poor (2.3–6.4%) for all catalysts. The apparent low

Table 4

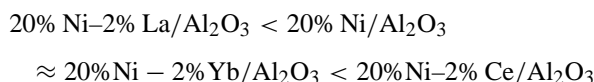
H₂ chemisorption data on various lanthanide-promoted sol–gel Ni/Al₂O₃ catalysts reduced under H₂ at 600 °C for 2 h

Catalyst	Percentage <i>D</i> ^a	MSA (m ² /g) ^b
20% Ni/Al ₂ O ₃	4.9	6.6
20% Ni–2% La/Al ₂ O ₃	3.7	4.9
20% Ni–5% La/Al ₂ O ₃	3.3	4.5
20% Ni–2% Ce/Al ₂ O ₃	6.4	8.5
20% Ni–5% Ce/Al ₂ O ₃	2.3	3.1
20% Ni–2% Yb/Al ₂ O ₃	5.0	6.6
20% Ni–5% Yb/Al ₂ O ₃	2.8	3.8

^a Percentage nickel dispersion.

^b Nickel surface area, m²/g.

nickel dispersion on the high surface area of sol–gel alumina could be due to the formation of NiAl₂O₄, which is rather difficult to reduce [29,30]. The amount of H₂ chemisorbed on pure sol–gel alumina is negligibly small, thus no correction on H₂ uptake values was made. The nickel dispersion and nickel surface area increase in the following order:



Additionally, the nickel dispersion and nickel surface area are seen to decrease at higher lanthanide content; a decrease is more pronounced with Ni–Ce/Al₂O₃ and Ni–Yb/Al₂O₃ catalysts. This implies that higher amounts of lanthanides could cover or block nickel sites for hydrogen adsorption.

The effect of calcination and reduction temperatures on the nickel dispersion and nickel surface area of Ni/Al₂O₃ and Ni–Ce/Al₂O₃ catalysts is further examined. As reported in Table 5, there are three major trends exhibited by the H₂ chemisorption data: (i) for the catalysts calcined at 450 °C, the nickel dispersion and nickel surface area increase with increasing reduction temperature and reach a maximum at 600 °C. Further increase in reduction temperature to 700 °C leads to a decrease in both parameters. It is conceivable that growth of nickel crystallites becomes more prominent with higher reduction temperatures; (ii) the nickel dispersion and nickel surface area increase with increasing reduction temperature for the catalysts calcined at 600 °C. In addition, the

Table 6

Propane steam reforming reaction data obtained with sol–gel Ni/Al₂O₃ catalysts—effect of synthesis parameters

Synthesis parameters			C ₃ H ₈ conversion (%)	H ₂ yield (%)	Selectivity (%)		
Ni content (wt.%)	pH	H ₂ O/ATB ratio			CO ₂	CH ₄	CO
10	4.8	3.6	16	21	85	0	15
15	4.8	3.6	27	33	73	19	8
20	4.8	3.6	53	37	54	36	10
25	4.8	3.6	43	29	52	31	17
20	4.8	3.6	53	37	54	36	10
20	7.0	3.6	31	28	61	20	19
20	8.8	3.6	27	26	68	20	12
20	4.8	3.6	53	37	54	36	10
20	4.8	4.0	43	30	63	30	7
20	4.8	5.0	23	23	77	15	8

Reaction conditions: 500 °C, C₃H₈/H₂O/N₂ = 1/4/95, feed flow rate = 300 cm³/min, equal surface area reactions (9 m²).

Table 5

Effect of calcination (*T*_{cal}) and reduction (*T*_{red}) temperatures on nickel dispersion and surface area of sol–gel 20% Ni/Al₂O₃ and 20% Ni–2% Ce/Al₂O₃ catalysts

Catalyst	<i>T</i> _{cal} (°C)	<i>T</i> _{red} (°C)	Percentage <i>D</i> ^a	MSA (m ² /g) ^b
20% Ni/Al ₂ O ₃	450	500	3.7	5.0
		600	4.9	6.6
		700	4.8	6.4
	600	500	3.3	4.4
		600	5.2	7.0
		700	5.4	7.2
20% Ni–2% Ce/Al ₂ O ₃	450	500	5.2	6.9
		600	6.4	8.5
		700	6.2	8.3
	600	500	3.8	5.0
		600	6.2	8.2
		700	6.7	8.9

^a Percentage nickel dispersion.

^b Nickel surface area, m²/g.

catalysts exhibit higher nickel dispersion and larger nickel surface area at the reduction temperature of 700 °C compared to those calcined at 450 °C; and (iii) regardless of calcination and reduction temperatures, Ni–Ce/Al₂O₃ catalysts possess higher nickel dispersion and larger nickel surface area than Ni/Al₂O₃ catalysts.

3.4. Catalytic activity

3.4.1. Effect of synthesis parameters

The effect of catalyst synthesis parameters on the catalytic activity of sol–gel Ni/Al₂O₃ catalysts at 500 °C and H₂O/C = 1.3 is shown in Table 6. The parameters examined are Ni content, pH, and H₂O/ATB ratio.

As reported in Table 6, C₃H₈ conversion and H₂ yield are seen to increase with increasing Ni content and reach a maximum at 20 wt.%, with C₃H₈ conversion and H₂ yield at 53 and 37%, respectively. Further increase in Ni content to 25 wt.% leads to a decline in catalytic activity. Moreover, the variations of pH and H₂O/ATB ratio also have a pronounced effect on catalytic activity of 20% Ni/Al₂O₃

catalysts. The selectivities to C-containing products are also shown in Table 6. The C-containing products from propane steam reforming are CO, CO₂, and CH₄ with CO₂ being the main one. CO₂ selectivity is seen to increase with a decrease in CH₄ selectivity at lower C₃H₈ conversions. No CH₄ formation is observed at 10 wt.-%.

3.4.2. Effect of lanthanide promotion

Several sol–gel 20% Ni/Al₂O₃ catalysts promoted with lanthanide elements (La, Ce, Yb) were subsequently prepared at pH = 4.8 and H₂O/ATB = 3.6. The influence of lanthanide promotion (2 wt.%) on catalytic performance at different reaction temperatures is shown in Fig. 4. C₃H₈ conversion (Fig. 4a) and H₂ yield (Fig. 4b) are seen to increase with increasing reaction temperature on all catalysts. Hydrogen yield that would be obtained at equilibrium is also included for comparison. 20% Ni–2% Ce/Al₂O₃ and 20% Ni–2% Yb/Al₂O₃ catalysts show an improvement in C₃H₈ conversion and H₂ yield compared to 20% Ni/Al₂O₃ catalyst. Although 20% Ni–2% La/Al₂O₃ catalyst exhibits similar C₃H₈ conversion to 20% Ni/Al₂O₃ catalyst, it still shows an increased H₂ yield above 450 °C. At 500 °C, the high-

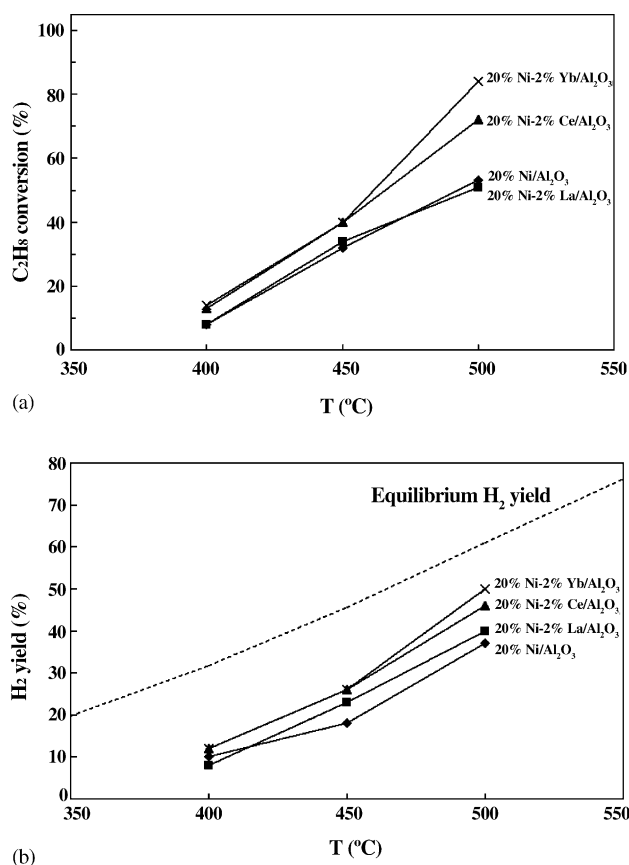


Fig. 4. Effect of reaction temperature on catalytic performance of lanthanide-promoted sol–gel 20% Ni/Al₂O₃ catalysts in propane steam reforming (a) C₃H₈ conversion (b) H₂ yield [reaction conditions: 400–500 °C, C₃H₈/H₂O/N₂ = 1/4/95, feed flow rate = 300 cm³/min, equal surface area reactions (9 m²)].

Table 7

Reaction comparison for propane steam reforming (dilution experiments) at 500 °C

Catalyst	C ₃ H ₈ conversion (%)	H ₂ yield (%)	Selectivity (%)		
			CO ₂	CH ₄	CO
20% Ni/Al ₂ O ₃	53	37	54	36	10
20% Ni–2% La/Al ₂ O ₃	51	40	59	28	13
20% Ni–5% La/Al ₂ O ₃	29	29	55	29	16
20% Ni–2% Ce/Al ₂ O ₃	72	46	50	38	12
20% Ni–5% Ce/Al ₂ O ₃	53	38	56	33	11
20% Ni–2% Yb/Al ₂ O ₃	84	50	46	38	16
20% Ni–5% Yb/Al ₂ O ₃	65	44	50	35	15

Reaction conditions: 500 °C, C₃H₈/H₂O/N₂ = 1/4/95, feed flow rate = 300 cm³/min, equal surface area reactions (9 m²).

est C₃H₈ conversion (84%) and H₂ yield (50%) are achieved with 20% Ni–2% Yb/Al₂O₃ catalyst. The effect of lanthanide promotion is more evident at higher reaction temperatures.

When the performances in propane steam reforming at different lanthanide contents are compared at 500 °C (Table 7), reaction data show that C₃H₈ conversion and H₂ yield decrease with increasing lanthanide content from 2 to 5 wt.-%. H₂ chemisorption data have also shown a decreasing trend of nickel surface area at higher lanthanide content. This indicates that the catalytic activity of lanthanide-promoted sol–gel Ni/Al₂O₃ catalysts is strongly related to nickel surface area. Thus, loss of activity with higher lanthanide content is due to the blockage of active sites by excess amounts of lanthanides introduced in the catalysts. It is noted that the distribution of C-containing products is not much affected by an increase in lanthanide content.

To further investigate catalytic performance at higher reaction temperature, steady-state reaction experiments were conducted at 550 °C. However, the feed flow rate was raised to 400 cm³ (STP)/min to avoid complete C₃H₈ conversion. Interestingly, the highest C₃H₈ conversion (80%) and H₂ yield (52%) are obtained with 20% Ni–2% Ce/Al₂O₃ catalyst at 550 °C (Table 8). Furthermore, 20% Ni–2% La/Al₂O₃ catalyst also shows a significant improvement in steam reforming activity compared to 20% Ni/Al₂O₃ catalyst under these reaction conditions. Moreover, an increase in CO selectivity is observed at higher reaction temperature. This suggests an increased contribution from the reverse water-gas shift reaction (CO₂ + H₂ → CO + H₂O) to the overall reaction network. Another possible explanation is that at higher

Table 8

Reaction comparison for propane steam reforming (dilution experiments) at 550 °C

Catalyst	C ₃ H ₈ conversion (%)	H ₂ yield (%)	Selectivity (%)		
			CO ₂	CH ₄	CO
20% Ni/Al ₂ O ₃	48	36	48	21	31
20% Ni–2% La/Al ₂ O ₃	66	52	38	25	37
20% Ni–2% Ce/Al ₂ O ₃	80	52	31	32	37
20% Ni–2% Yb/Al ₂ O ₃	70	50	33	30	37

Reaction conditions: 550 °C, C₃H₈/H₂O/N₂ = 1/4/95, feed flow rate = 400 cm³/min, equal surface area reactions (9 m²).

conversion, water becomes the limiting reactant, and leading to an increased formation of CO as opposed to CO₂ from the steam reforming reaction. Increased coking on the surface at higher temperatures could also lead to higher CO formation through the gasification of surface carbon.

“Neat” experiments were performed with 20% Ni/Al₂O₃, 20% Ni–2% Ce/Al₂O₃, and 20% Ni–2% Yb/Al₂O₃ catalysts in propane steam reforming without N₂ dilution at the following conditions: $T = 500\text{--}550\text{ }^{\circ}\text{C}$, $\text{H}_2\text{O}/\text{C} = 4$, total feed rate = 270 cm^3 (STP)/min, equal surface area reaction (18 m^2). Demineralized distilled water was delivered by an Eldex metering pump (model: A-10-S) connected with a 40 psi back pressure regulator and subsequently vaporized in a preheater which was operated above $150\text{ }^{\circ}\text{C}$. A column packed with ceramic beads was installed after the preheater to help C₃H₈ and steam mix effectively. The steady-state reaction experiments were performed using 1/2 in. o.d. stainless steel flow reactor to avoid high pressure drop due to higher amounts of catalysts loaded in the reactor. Consistent with reaction data obtained from dilution experiments, lanthanide-promoted catalysts give higher C₃H₈ conversion and H₂ yield compared to the unpromoted catalyst (Table 9).

3.4.3. Effect of calcination and reduction temperatures

When the effect of reduction temperature was examined by keeping the calcination temperature constant at $450\text{ }^{\circ}\text{C}$, a maximum is observed at a reduction temperature of $600\text{ }^{\circ}\text{C}$ (Fig. 5). Both 20% Ni/Al₂O₃ and 20% Ni–2% Ce/Al₂O₃ catalysts give the highest H₂ yield when reduced at $600\text{ }^{\circ}\text{C}$. However, 20% Ni–2% Ce/Al₂O₃ catalyst gives superior performance at every reduction temperature. An improvement in H₂ yield with cerium promotion is much more evident at higher reduction temperatures. Furthermore, the catalytic activity of both catalysts calcined at $450\text{ }^{\circ}\text{C}$ is seen to go

Table 9

Reaction comparison for propane steam reforming (neat experiments)

Catalyst	T ($^{\circ}\text{C}$)	C ₃ H ₈ conversion (%)	H ₂ yield (%)	Selectivity (%)		
				CO ₂	CH ₄	CO
20% Ni/Al ₂ O ₃	500	35	14	68	25	7
	550	43	18	69	20	11
20% Ni–2%Ce/Al ₂ O ₃	500	43	15	65	28	7
	550	95	31	58	28	14
20% Ni–2%Yb/Al ₂ O ₃	500	59	19	60	32	8
	550	83	27	58	30	12

Reaction conditions: $500\text{--}550\text{ }^{\circ}\text{C}$, $\text{H}_2\text{O}/\text{C} = 4$, total feed rate = 270 cm^3 /min, equal surface area reaction (18 m^2).

through a maximum at the reduction temperature of $600\text{ }^{\circ}\text{C}$ and decreases at higher reduction temperature. By comparing the performance of 20% Ni–2% Ce/Al₂O₃ catalysts calcined at 450 and $600\text{ }^{\circ}\text{C}$, we see that higher calcination temperature causes a decline in catalytic activity (Fig. 5b). The optimum reduction temperature is $600\text{ }^{\circ}\text{C}$ regardless of calcination temperature. This observation is in good agreement with TPR results. When Ni–Ce/Al₂O₃ catalysts are calcined at higher temperature ($600\text{ }^{\circ}\text{C}$), NiO interacts with Al₂O₃ to form a very stable NiAl₂O₄ spinel which is more difficult to reduce [31–35]. However, we cannot explain the lower activity of the catalyst calcined at $600\text{ }^{\circ}\text{C}$ when it is reduced at $700\text{ }^{\circ}\text{C}$. As previously discussed, the catalysts calcined at higher temperature exhibit higher nickel dispersion and nickel surface area when reduced at $700\text{ }^{\circ}\text{C}$ (Table 5). Our in situ X-ray diffraction studies performed to observe the phase changes during reduction have shown incomplete reduction at lower temperatures while Ni sintering was observed at higher temperatures [36].

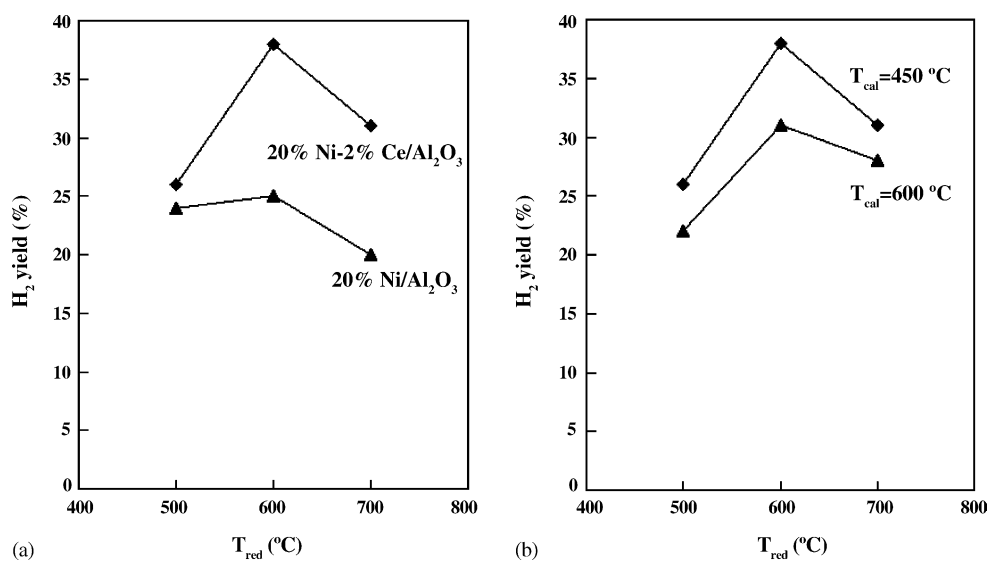


Fig. 5. Effect of calcination and reduction temperatures on catalytic performance in propane steam reforming (a) comparison between 20% Ni/Al₂O₃ and 20% Ni–2% Ce/Al₂O₃ catalysts calcined at $450\text{ }^{\circ}\text{C}$; (b) effect of calcination temperature on 20% Ni–2% Ce/Al₂O₃ catalysts [reaction conditions: $550\text{ }^{\circ}\text{C}$, $\text{H}_2\text{O}/\text{C} = 2$, $\text{GHSV} = 248,000\text{ h}^{-1}$].

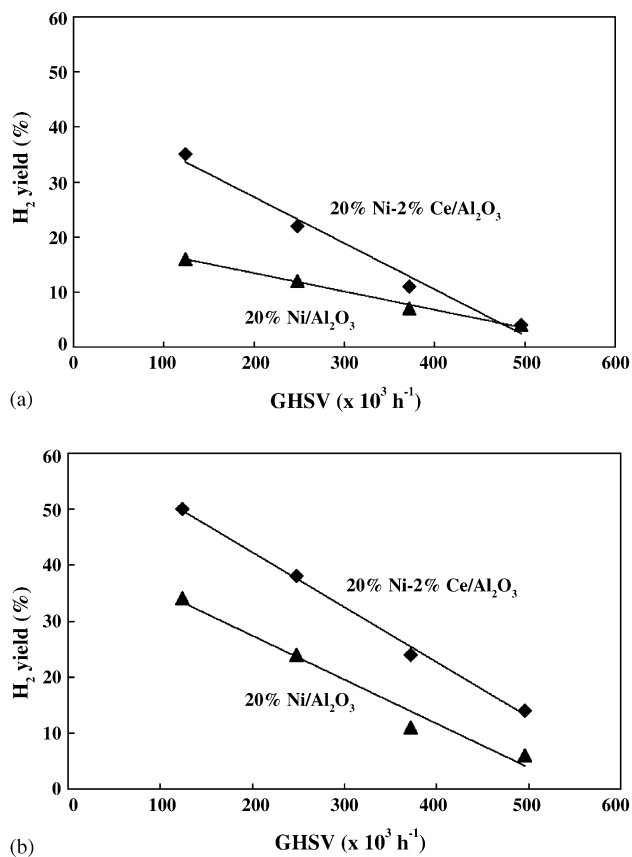


Fig. 6. Effect of GHSV on H_2 yield in propane steam reforming over 20% Ni/ Al_2O_3 and 20% Ni–2% Ce/ Al_2O_3 catalysts: (a) 500 °C and (b) 550 °C.

3.4.4. Effect of gas hourly space velocity (GHSV)

The catalytic performance of 20% Ni/ Al_2O_3 and 20% Ni–2% Ce/ Al_2O_3 catalysts in propane steam reforming was further investigated at various space velocities. The reaction conditions for these experiments were as follows: 500–550 °C, $H_2O/C = 2$. The variation of GHSV was performed by adjusting both the amount of the catalyst (10–20 mg) and the feed flow rate (200–400 cm^3 (STP)/min). As expected, H_2 yield increases with decreasing GHSV from 496,000 to 124,000 h^{-1} over both catalysts (Fig. 6). At 500 °C, the beneficial effect of cerium promotion becomes much more pronounced at lower GHSVs. At 550 °C, an improvement in H_2 yield with the addition of cerium is evident for the whole range of GHSVs examined. C_3H_8 conversion rates at steady state were further normalized to surface nickel atoms, measured by H_2 chemisorption at 35 °C, in the form of turnover frequencies (TOFs). Table 10 compares average TOFs obtained with 20% Ni/ Al_2O_3 and 20% Ni–2%

Table 10
Effect of reaction temperature on turnover frequency

Catalyst	TOF (s^{-1})	
	500 °C	550 °C
20% Ni/ Al_2O_3	0.35	0.65
20% Ni–2%Ce/ Al_2O_3	0.50	1.20

Table 11
Comparison of CO-methanation activity of 20% Ni/ Al_2O_3 and 20% Ni–2% Ce/ Al_2O_3 catalysts

Catalyst	CH ₄ yield (%)		CO ₂ yield (%)	
	500 °C	550 °C	500 °C	550 °C
20% Ni/ Al_2O_3	59	46	5	5
20% Ni–2%Ce/ Al_2O_3	71	61	5	5

Reaction conditions: $F_{CO} = 10 cm^3$ (STP)/min, $CO_2/H_2/N_2 = 1/6/13$, $GHSV = 372,000 h^{-1}$.

Ce/ Al_2O_3 catalysts at 500 and 550 °C. TOF is seen to increase with increasing reaction temperature. The increase is more pronounced with 20% Ni–2% Ce/ Al_2O_3 catalyst. Furthermore, the higher activity of promoted catalysts is clearly seen when TOF values are compared for the 20% Ni–2% Ce/ Al_2O_3 and 20% Ni/ Al_2O_3 catalysts.

The variation of product selectivities with C_3H_8 conversion over 20% Ni/ Al_2O_3 and 20% Ni–2% Ce/ Al_2O_3 catalysts is shown in Fig. 7. In this study, CO_2 selectivity is defined as the ratio of moles of CO_2 produced to the total moles of C-containing products (i.e., CO_2 , CO, and CH_4) whereas H_2 selectivity is defined as $2 \times$ moles of H_2 produced/total moles of hydrogen in the H-containing products, which are H_2 and CH_4 . Interestingly, CH_4 selectivity is seen to increase at the expense of both H_2 and CO_2 selectivities at lower GHSVs, i.e., higher conversions. This suggests that CO_2 methanation ($CO_2 + 4H_2 \rightarrow CH_4 + 2H_2O$) becomes more appreciable when residence time is increased, leading to an increased CH_4 selectivity. CO selectivity, on the other hand, is not much affected by the variation of C_3H_8 conversion over either catalyst.

The CO- and CO_2 -methanation reactions over 20% Ni/ Al_2O_3 and 20% Ni–2% Ce/ Al_2O_3 catalysts were further investigated at 500–550 °C. The H_2/CO and H_2/CO_2 ratios for these experiments were kept constant at 6. CH_4 yield is defined as moles of carbon in CH_4 produced/total moles of carbon in the feed. As shown in Tables 11 and 12, CH_4 yield is seen to decrease with increasing reaction temperature over both catalysts. Ce-promoted catalyst shows higher CH_4 yields from both CO- and CO_2 -methanation reactions compared to unpromoted catalyst. It is worth noting that a lower level of CH_4 produced from the CO_2 -methanation reaction at 550 °C implies an increased contribution from the reverse water-gas shift reaction at higher temperature. Ross and co-workers [37,38] studied the CO-methanation reaction

Table 12
Comparison of CO_2 -methanation activity of 20% Ni/ Al_2O_3 and 20% Ni–2% Ce/ Al_2O_3 catalysts

Catalyst	CH ₄ yield (%)		CO yield (%)	
	500 °C	550 °C	500 °C	550 °C
20% Ni/ Al_2O_3	14	13	28	36
20% Ni–2%Ce/ Al_2O_3	30	22	24	34

Reaction conditions: $F_{CO_2} = 15 cm^3$ (STP)/min, $CO_2/H_2/N_2 = 1/6/20$, $GHSV = 496,000 h^{-1}$.

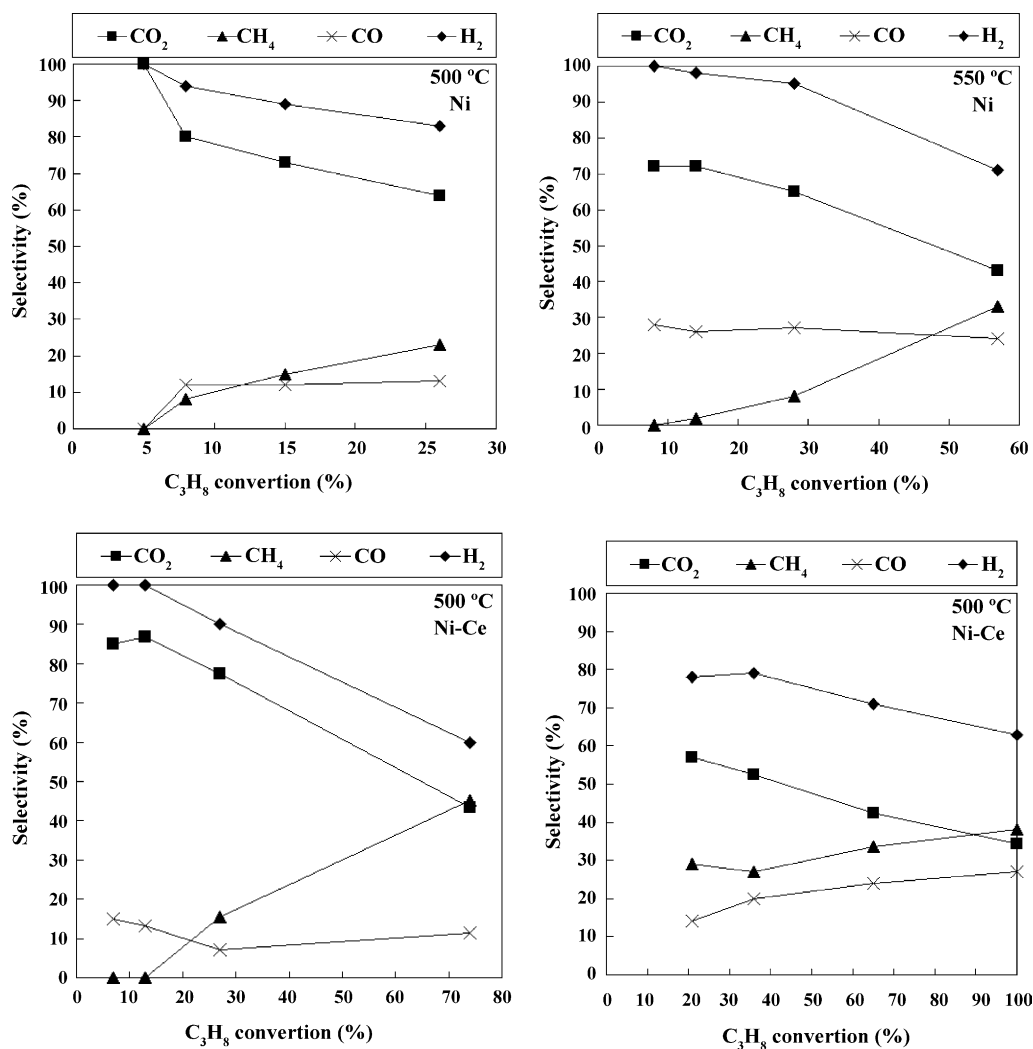


Fig. 7. Variation of product selectivities with C₃H₈ conversion.

on coprecipitated Ni/Al₂O₃ catalysts promoted with La₂O₃ and CeO₂. An enhancement in methanation activity was observed with an increase in apparent activation energy upon lanthanide promotion. The role of lanthanum and cerium in the methanation reaction was reported to be associated with higher amounts of CO and H₂ adsorbed on nickel surface due to an interaction between lanthanides and nickel in the catalysts. Our H₂ chemisorption studies have shown that 20% Ni–2% Ce/Al₂O₃ catalyst shows an increased H₂ uptake compared to 20% Ni/Al₂O₃ catalyst, thus resulting in higher nickel dispersion and larger nickel surface area (Table 4). Furthermore, the CO uptakes measured by CO chemisorption at 35 °C are 3.39 and 10.16 cm³/g_{cat} over 20% Ni/Al₂O₃ and 20% Ni–2% Ce/Al₂O₃ catalysts reduced at 600 °C, respectively. Consequently, an improvement in methanation activity when cerium is added into sol–gel Ni/Al₂O₃ catalysts could be due to an increased CO and H₂ adsorption on nickel crystallites. A higher amount of CO₂ adsorbed on nickel upon cerium promotion could also be another possibility.

3.5. DRIFTS studies

3.5.1. C₃H₈-TPD/TPReaction

TPD/TPReaction experiments with DRIFTS were performed over reduced 20% Ni–2% Ce/Al₂O₃ catalyst, where strongly adsorbed propane was allowed to react with water. Adsorption of propane was carried out at room temperature for 1 h. The system was subsequently purged and heated under He and spectra were collected in steps under He flow up to 450 °C. The introduction of H₂O was performed at 450 °C for different times on stream (i.e., 5, 10, and 15 min) followed by He flushing before spectra were taken.

Fig. 8 shows DRIFT spectra taken at 25, 100, 200, 250, 300, and 450 °C under He after C₃H₈ adsorption over reduced 20% Ni–2% Ce/Al₂O₃ catalyst. After propane adsorption and He flushing, bands remained at 2940, 2932 (shoulder), 2824, 1630, 1476, 1435 (shoulder), 1373, 1189, and 1103 cm⁻¹ at room temperature. The band at 1630 cm⁻¹ could be attributed to an olefinic C=C vibration [39,40]

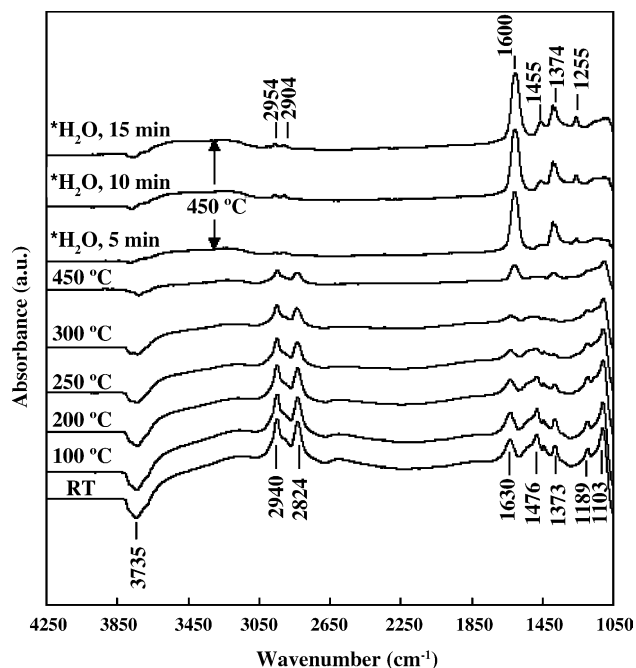


Fig. 8. DRIFT spectra taken over reduced 20% Ni–2% Ce/Al₂O₃ catalysts after C₃H₈ adsorption; *H₂O was introduced for 5, 10, and 15 min and the system was flushed under He for 5 min.

and has been observed in a separate propylene adsorption/desorption DRIFTS experiment performed in our laboratory (Fig. 9). However, bands typical of olefinic sp² C–H stretching present above 3000 cm⁻¹ were not observed after propane adsorption which leads us to assume that the band at 1630 cm⁻¹ could be assigned as the O–H bending frequency of adsorbed water as observed by Gates and co-workers [41]. The remaining bands are characteristic of adsorbed propylidyne [39,42] and are similar to resultant spectra of propane adsorbed on a reduced Ir/Al₂O₃ catalyst [41]. In addition, a

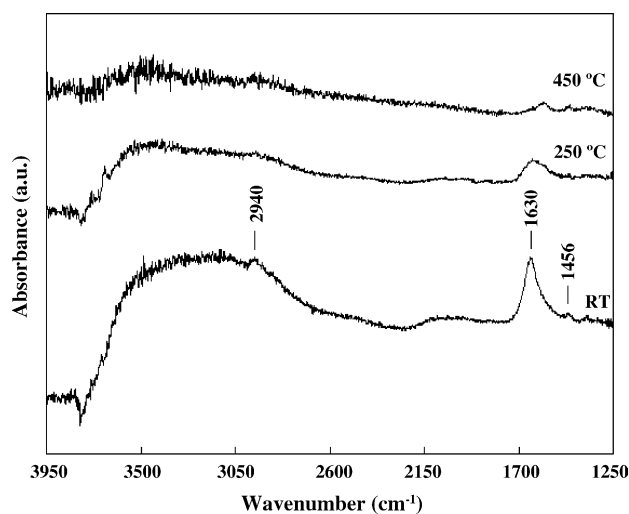


Fig. 9. DRIFT spectra taken over reduced 20% Ni–2% Ce/Al₂O₃ catalysts after C₃H₆ adsorption at room temperature.

negative peak at 3750 cm⁻¹, which is characteristic of surface hydroxyl groups on the alumina support, was observed [43,44]. This indicates that the surface hydroxyl groups either interacted with propane or were consumed upon the adsorption of propane. Although the intensities of the bands at 2940 and 2824 cm⁻¹ decreased at higher temperatures, they were thermally stable up to 450 °C. The features at 2940 and 2932 cm⁻¹ are assigned to asymmetric CH₃ stretching [$\nu_{as}(\text{CH}_3)$] and asymmetric CH₂ stretching [$\nu_{as}(\text{CH}_2)$], respectively [39,42, 45–47]. The feature at 2824 cm⁻¹ could be attributed to either symmetric CH₂ stretching [$\nu_s(\text{CH}_2)$] or symmetric CH₃ stretching [$\nu_s(\text{CH}_3)$] [42,48]. The features at 1476, 1437, 1373, 1189, and 1103 cm⁻¹ decreased in intensity with temperature and subsequently almost disappeared at 300 °C. These features could be associated with adsorbed ethylidyne/propylidyne species that were depleted upon the reaction with H₂O. At 450 °C and before the introduction of water, new bands at 1600 and 1374 cm⁻¹ were present accompanied by two small C–H stretching bands at 2954 and 2904 cm⁻¹. Although it is conceivable that new CH₃ groups could be forming due to desorption/re-adsorption processes, a more likely explanation is that the features at 2954, 2904, 1600, and 1374 cm⁻¹ are due to formate species [49,50]. With the introduction of water at 450 °C, the bands associated with the formate species grew much stronger and were seen in higher intensity with time on stream. In the course of propane steam reforming, formate species are probably produced by the reaction of CO with the water introduced. In the absence of water, surface hydroxyl groups can serve as a source of oxygen to form formate species. Our formate band assignments are consistent with those which arise from adsorption of CO on 1% Au/ceria and 1% Pt/ceria catalysts [51]. Two additional features at 1455 and 1255 cm⁻¹, which could be attributed to carbonate species, were also observed after H₂O exposure at 450 °C [49,50].

In order to help in the band assignments for the C₃H₈-TPD/TPReaction experiment, DRIFT spectra were taken after propylene and CO₂ adsorption in separate experiments. Fig. 9 shows DRIFT spectra taken at 25, 250, and 450 °C under He flow over reduced 20% Ni–2% Ce/Al₂O₃ catalyst during the C₃H₆-TPD experiment. The strong presence of the band at 1630 cm⁻¹ on the catalyst surface following propylene adsorption signals the C=C stretching vibration. Presence of olefinic C–H vibrations that would be expected above 3000 cm⁻¹ cannot be discerned from this spectrum due to a very broad feature in that region. It is possible that adsorbed propylene could be dehydrogenated on the surface, giving rise to water (surface hydroxyl groups), which would show an IR band around 1630 cm⁻¹ as well as a broad feature above 3000 cm⁻¹. The feature at 1373 cm⁻¹, which was quite prominent following propane adsorption, could not be observed after propylene adsorption. This observation supports the assignment of the band at 1373 cm⁻¹ to symmetric CH₃ bending [$\delta_s(\text{CH}_3)$] of propylidyne. This assignment is in agreement with what is reported by Shahid and Sheppard [42]. In addition, the feature at 2824 cm⁻¹ was absent,

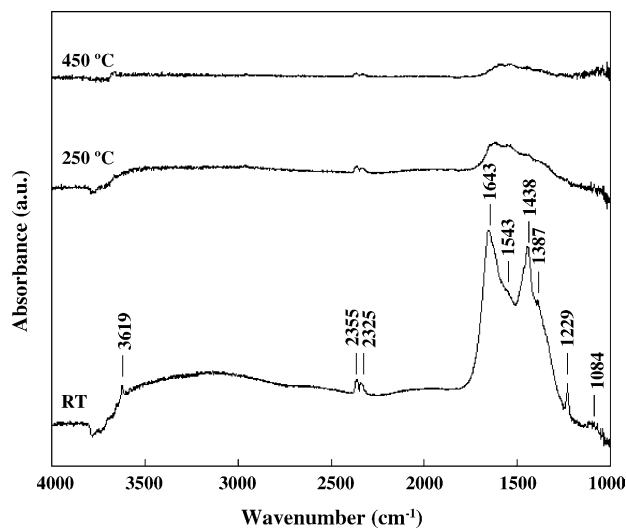


Fig. 10. DRIFT spectra taken over reduced 20% Ni–2% Ce/Al₂O₃ catalysts after CO₂ adsorption at room temperature.

and the 2940 cm⁻¹ band was much weaker and disappeared very quickly at higher temperatures. The band at 1476 cm⁻¹, which was quite strong following propane adsorption was barely noticeable (~1456 cm⁻¹) after propylene adsorption. This observation makes us believe that this feature could be due to a methyl group, which may have a different orientation in species resulting from propylene adsorption. This explanation would also be consistent with our earlier assertion that propylidyne species are the predominant hydrocarbon derivatives on the surface following propane adsorption, but this is not necessarily the case following propylene adsorption.

From DRIFT spectra of CO₂-TPD over the reduced 20% Ni–2% Ce/Al₂O₃ catalyst, bands at 3619, 2355, 2325, 1643, 1543 (shoulder), 1438, 1387 (shoulder), 1229, and 1084 cm⁻¹ are seen at room temperature (Fig. 10). The bands at 3619, 1643, 1438, and 1229 cm⁻¹ are assigned to bicarbonate species and decrease in intensity significantly at 250 °C [49,50,52]. Conversely, carbonate species are characterized by the shoulder bands at 1543, and 1387 cm⁻¹ as well as the 1084 cm⁻¹ band [49,50,52]. In addition, the only other feature observed is a doublet at 2355 and 2325 cm⁻¹, which corresponds to adsorbed CO₂ [53,54]. The disappearance of carbonate and bicarbonate species at higher temperatures leads us to believe that formate and carbonate species observed from the C₃H₈-TPD/TPReaction experiment are the result of the surface transformation of propylidyne species rather than from the re-adsorption of CO₂.

3.5.2. C₃H₈ + H₂O-TPReaction

C₃H₈ + H₂O-TPReaction with DRIFTS was also performed over reduced 20% Ni–2% Ce/Al₂O₃ catalyst. C₃H₈ was adsorbed at room temperature for 1 h. The system was then purged under He for 30 min and H₂O was subsequently introduced for 5 min at room temperature followed by He flushing for 5 min. The system was heated and DRIFT spec-

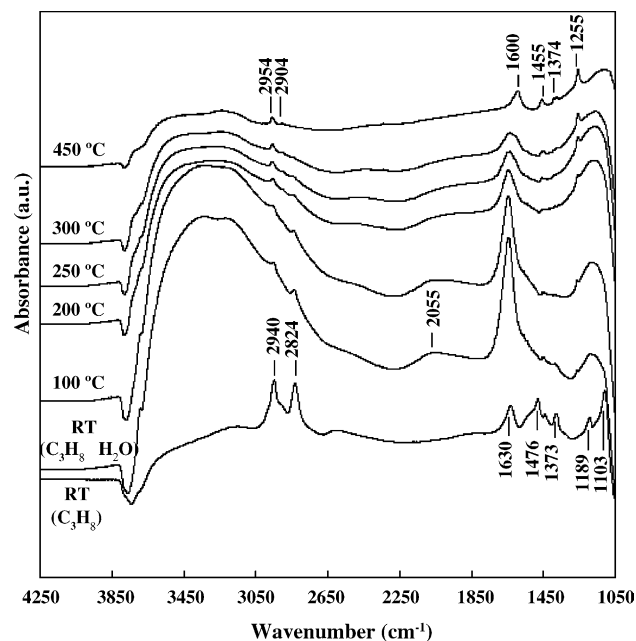


Fig. 11. DRIFT spectra taken over reduced 20% Ni–2% Ce/Al₂O₃ catalysts after consecutive adsorption of C₃H₈ and H₂O.

tra were collected in steps under He flow up to 450 °C. It is noted that H₂O was re-introduced at each temperature for 5 min followed by He flushing before taking spectra.

After C₃H₈ and H₂O introduction at room temperature, bands remained at 3750–3500 (very broad), 2940, 2824, 2055, 1630, 1435 (weak), 1373 (weak), and 1255 (weak) cm⁻¹ (Fig. 11). The broad band around 3750–3500 cm⁻¹ is characteristic of the OH stretching region while the feature at 2055 cm⁻¹ is assigned to linearly adsorbed CO on the catalyst surface and disappeared above 200 °C [55–57]. Compared to the DRIFT spectrum after C₃H₈ adsorption at room temperature, the intensity of the band located at 1630 cm⁻¹ increased significantly when H₂O was introduced at room temperature. This band decreased in intensity at higher temperatures and eventually shifted to 1600 cm⁻¹ at 450 °C. The band at 1600 cm⁻¹ is attributed to a formate species as previously observed from the C₃H₈-TPD/TPReaction experiment. The features at 2940 and 2824 cm⁻¹ were seen in much lower intensity and disappeared above 250 °C whereas the bands at 2954 and 1455 cm⁻¹ started to appear at 200 °C and grew stronger at higher temperatures. Furthermore, two additional bands at 2904 and 1374 were seen at 450 °C. It is evident that most surface species such as formate and carbonate ions are formed upon the reaction of adsorbed C₃H₈ and H₂O above 250 °C. In a separate experiment with C₃H₈ + H₂O adsorption in a reverse order (not shown), a large band at 1645 cm⁻¹ was also observed after water adsorption at room temperature. This observation provides additional support for our earlier assertion that the 1630 cm⁻¹ feature seen in the C₃H₈-TPD/TPReaction and C₃H₈ + H₂O-TPReaction experiments is due to adsorbed water. Interestingly, no additional features

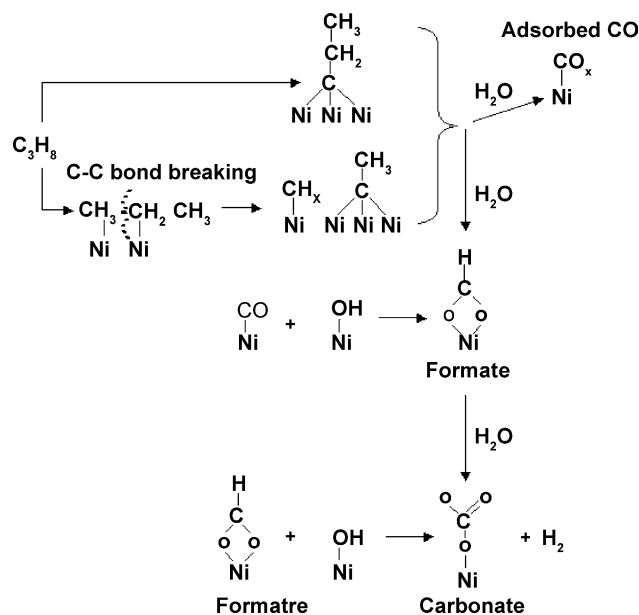


Fig. 12. Possible mechanistic steps during propane steam reforming over reduced Ni-Ce/Al₂O₃ catalyst as observed using in situ DRIFTS.

were seen following C_3H_8 adsorption, suggesting water could be primarily adsorbed on metallic nickel sites and therefore inhibits the adsorption of propane.

Based on the observed surface species transformations from in situ DRIFTS studies, the following major reaction pathways for adsorbed propane in the presence of steam over reduced sol-gel Ni-Ce/Al₂O₃ catalysts are proposed as illustrated in Fig. 12. The first step is believed to be adsorption of propane on metallic nickel sites to form propylidyne. To a lesser degree, adsorbed propane can further decompose into hydrocarbon fragments (i.e., CH_x) and even carbon oxides in the presence of adsorbed water. Carbon deposition, especially at higher temperatures, also is a possibility as seen through our coking studies [36]. During this step, it is likely that the formation of carbon monoxide could be occurring on nickel sites. Adsorbed water from the catalyst can combine with adsorbed hydrocarbon fragments or adsorbed carbon monoxide to form formate species. It is also possible that adsorbed hydrocarbon fragments could react with other sources of oxygen (hydroxyls, ceria lattice) to form formates in the absence of water, as observed at 450 °C (Fig. 8). Additionally, it is possible that water could dissociatively adsorb to produce gaseous hydrogen and surface oxygen species. These surface oxygen species have been found to react with methane to form CO and hydrogen in methane steam reforming over various oxide supports, including ceria [58–60]. Unfortunately, we cannot obtain information pointing to the dissociative adsorption of water to form hydrogen from the DRIFTS experiments. However, the contribution from hydroxyls created from adsorbed water is expected to be much higher than that from surface oxygen. The thermal decomposition of adsorbed formates can result in the formation of carbon dioxide and hydrogen, or the formation of carbon monoxide and

hydroxyl groups [50]. Moreover, the fraction of the formate remaining adsorbed could react with hydroxyl groups arising from adsorbed water to form carbonates and hydrogen at higher temperatures. While the DRIFTS experiments do not specifically indicate the participation of other surface intermediates, it could be possible that adsorbed species such as oxygen atoms, hydrogen atoms, and hydroxyl groups could also be spilling over to the nickel surface from the alumina support or ceria, thus enhancing the overall adsorption and participation of water.

4. Conclusions

Various sol-gel Ni/Al₂O₃ catalysts promoted with lanthanide elements (La, Ce, and Yb) were studied in the steam reforming of propane. The promotion effect is most pronounced on the Ni-Ce/Al₂O₃ catalysts. An improvement in catalytic activity with respect to C_3H_8 conversion and H_2 yield appears to be due to easier reduction of nickel species to a metallic state and larger nickel surface area. Additionally, cerium promotion enhances the CO- and CO₂-methanation activity, leading to an increased CH_4 yield. DRIFT experiments suggest adsorbed propylidyne to be the predominant surface species following C_3H_8 adsorption at room temperature and to subsequently react with hydroxyl groups arising from adsorbed water to form formate and carbonate species at higher temperatures. The second paper of this series [36] examines the effect of lanthanide promotion in terms of the deactivation characteristics of these catalysts under steam reforming conditions.

Acknowledgments

The financial support provided by Honda Research Institute, USA Inc. and the National Science Foundation (NSF-DMR grant # 0114098) is gratefully acknowledged. The authors thank Dr. Rick B. Watson for his helpful discussion of the DRIFTS studies.

References

- [1] J.N. Armor, Appl. Catal. A 176 (1999) 159.
- [2] D.E. Ridler, M.V. Twigg, in: M.V. Twigg (Ed.), Catalyst Handbook, Wolfe, London, 1989, p. 225.
- [3] J.T. Richardson, S.A. Paripatyadar, Appl. Catal. A 61 (1990) 293.
- [4] A. Igarashi, T. Ohtaka, S. Motoki, Catal. Lett. 13 (1991) 189.
- [5] J.R. Rostrup-Nielsen, J.H. Hansen, J. Catal. 144 (1993) 38.
- [6] D. Qin, J. Lapszewicz, Catal. Today 21 (1994) 551.
- [7] R. Craciun, B. Shereck, R.J. Gorte, Catal. Lett. 51 (1998).
- [8] X. Wang, R.J. Gorte, Catal. Lett. 73 (2001) 15.
- [9] Q. Zhuang, Y. Qin, L. Chang, Appl. Catal. 70 (1991) 1.
- [10] B.L. Su, S.D. Guo, in: B. Delmon, G.F. Froment (Eds.), Catalyst Deactivation, Elsevier, Amsterdam, 1999, p. 325.
- [11] R.M. Sambrook, J.R.H. Ross, US Patent 4 469 815, 1984.
- [12] Z. Cheng, Q. Wu, J. Li, Q. Zhu, Catal. Today 30 (1996) 147.

- [13] S. Wang, G.Q. Lu, *Appl. Catal. B* 19 (1998) 267.
- [14] S. Wang, G.Q. Lu, *J. Chem. Technol. Biotechnol.* 75 (2000) 589.
- [15] J.A. Montoya, E.R. Pascual, C. Gimon, P.D. Angel, A. Monzon, *Catal. Today* 63 (2000) 71.
- [16] R. Zhang, F. Li, Q. Shi, L. Luo, *Appl. Catal. A* 205 (2001) 279.
- [17] U.S. Ozkan, Y. Cai, M.W. Kumthekar, L. Zhang, *J. Catal.* 142 (1993) 182.
- [18] R.D. Gonzalez, T. Lopez, R. Gomez, *Catal. Today* 35 (1997) 293.
- [19] Y.G. Chen, J. Ren, *Catal. Lett.* 29 (1994) 39.
- [20] C.E. Quincoces, S. Dicundo, A.M. Alvarez, M.G. Gonzalez, *Mater. Lett.* 50 (2001) 21.
- [21] Y.J. Huang, J.A. Schwarz, J.R. Diehl, J.P. Baltrus, *Appl. Catal.* 36 (1988) 163.
- [22] K.T. Ng, D.M. Hercules, *J. Phys. Chem. A* 80 (1976) 2094.
- [23] J.F. Moulder, W.F. Stickle, P.E. Sobol, K.D. Bomben, in: J. Chastain (Ed.), *Handbook of X-ray Photoelectron Spectroscopy*, Perkin-Elmer, Minnesota, 1992.
- [24] A. Velon, I. Olefjord, *Oxid. Met.* 56 (2001) 415.
- [25] X. Wang, U.S. Ozkan, *J. Phys. Chem. B* 109 (2005) 1882.
- [26] C.H. Bartholomew, R.J. Farrauto, *J. Catal.* 45 (1976) 41.
- [27] C.H. Bartholomew, R.B. Pannell, *J. Catal.* 65 (1980) 390.
- [28] R.J. Farrauto, C.H. Bartholomew, *Fundamentals of Industrial Catalytic Processes*, Blackie Academic & Professional, London, 1997.
- [29] Z. Zhang, X.E. Verykios, *Appl. Catal. A* 138 (1996) 109.
- [30] R.G. Ding, Z.F. Yan, *Catal. Today* 68 (2001) 135.
- [31] J.R.H. Ross, M.C.F. Steel, A. Zeini-Isfahani, *J. Catal.* 52 (1978) 280.
- [32] J. Zielinski, *J. Mol. Catal.* 83 (1993) 197.
- [33] J. Zielinski, *Appl. Catal. A* 94 (1993) 107.
- [34] C. Li, Y.W. Chen, *Thermo. Acta* 256 (1995) 457.
- [35] B. Vos, E. Poels, A. Bliet, *J. Catal.* 198 (2001) 77.
- [36] S. Natesakhawat, R.B. Watson, X. Wang, U.S. Ozkan, *J. Catal.*, in press.
- [37] H.G.J.L. Rotgerink, R.P.A.M. Paalman, J.G. Ommen, J.R.H. Ross, *Appl. Catal.* 45 (1988) 257.
- [38] H.G.J.L. Rotgerink, R.P.A.M. Paalman, J.G. Ommen, J.R.H. Ross, *Appl. Catal.* 45 (1988) 281.
- [39] F. Solymosi, R. Nemeth, L. Ovari, L. Egri, *J. Catal.* 195 (2000) 316.
- [40] M.A. Chesters, C.D.L. Cruz, P. Gardner, E.M. McCash, P. Pudney, G. Shahid, N. Sheppard, *J. Chem. Soc. Faraday Trans.* 86 (1990) 2757.
- [41] A.M. Argo, J.F. Goellner, B.L. Philips, G.A. Panjabi, B.C. Gates, *J. Am. Chem. Soc.* 123 (2001) 2275.
- [42] G. Shahid, N. Sheppard, *Spectrochimica Acta* 46A (1990) 999.
- [43] D.H. Lee, R.A. Condrate, *Mater. Lett.* 23 (1995) 241.
- [44] A. Hinz, M. Skoglundh, E. Fridell, A. Andersson, *J. Catal.* 201 (2001) 247.
- [45] N. Sheppard, C.D.L. Cruz, *Adv. Catal.* 41 (1996) 1.
- [46] P.D. Holmes, G.S. McDougall, I.C. Wilcock, *Catal. Today* 9 (1991) 15.
- [47] K. Nakamoto, *Infrared and Raman Spectra of Inorganic and Coordination Compounds*, third ed., John Wiley & Sons, 1978.
- [48] F.C. Tompkins, *Chemisorption of Gases on Metals*, Academic Press, 1978.
- [49] V.F. Kiselev, O.V. Krylov, *Adsorption and Catalysis on Transition Metals and Their Oxides*, Berlin, vol. 9, 1989.
- [50] D. Bianchi, T. Chafik, M. Khalfallah, S. Jean, *Appl. Catal. A* 105 (1993) 223.
- [51] G. Jacobs, P.M. Patterson, L. Williams, E. Chenu, D. Sparks, G. Thomas, B.H. Davis, *Appl. Catal. A* 262 (2004) 177.
- [52] R. Philip, K. Fujimoto, *J. Phys. Chem. A* 96 (1992) 9035.
- [53] M.A. Bollinger, M.A. Vannice, *Appl. Catal. B* 8 (1996) 417.
- [54] V. Ermini, E. Finocchio, S. Sechi, G. Busca, S. Rossini, *Appl. Catal. A* 190 (2000) 157.
- [55] S.I. Fujita, M. Nakamura, T. Doi, N. Takezawa, *Appl. Catal. A* 104 (1993) 87.
- [56] J. Ryczkowski, *Catal. Today* 68 (2001) 263.
- [57] D. Liu, G.H. Que, Z.X. Wang, Z.F. Yan, *Catal. Today* 68 (2001) 155.
- [58] K. Hou, R. Hughes, *Chem. Eng. J.* 82 (2001) 311.
- [59] Y. Matsumura, T. Nakamori, *Appl. Catal. A* 258 (2004) 107.
- [60] E. Ramirez-Cabrera, A. Atkinson, D. Chadwick, *Appl. Catal. B* 47 (2004) 127.